Structural Eng. / Earthquake Eng. Vol. 6. No. 2, 375s-386s. October 1989
Japan Society of Civil Engineers (Proc. of JSCE No. 410/I-12)

IN-PLANE ULTIMATE STRENGTH OF DECK-TYPE FIXED-END ARCH BRIDGES

By Tetsuya YABUKI and Shigeru KURANISHI***

Fixed-end restraint effect of arch ribs on the over-all, in-plane ultimate strength of deck type steel arch bridges is studied by an accurate nonlinear finite element approach. This approach takes into consideration the two important factors on nonlinearities, namely, geometric and material. The interaction between bending moment and axial thrust, the changes in deflection mode, and the progress of yielding and unloading zones with load level until the ultimate state are throughly examined. The load-deflection behavior, until the stability limit load is reached, has also been analyzed by elastic theory. Special characteristics of the local member failure of arch rib between the posts are finally investigated.

Keywords : *arch bridge, steel structure, compression member, structural stability*

1. INTRODUCTION

As main members of arch bridges are in combined compression and bending, their ultimate strengths are characterized by instability failing with the effect of nonlinearities due to both the change of geometry and yielding of material. These nonlinear behavior is receiving increasing attention following the move towards ultimate strength design concepts. Several researches have been made on inplane ultimate strength of deck-type, two-hinged steel arch bridge systems so far[1),2)] and considerable findings concerning them have been summarized by Ref. 3). Through these studies, characteristics of the ultimate strength of the hinged arch bridge system are fundamentally understood. Data on elastic instability of this type bridge systems have also presented recently[4)]. Very few researches, however, have been reported so far on the ultimate strengths of fixed-end arch bridge systems and the most past works on them have dealt with arch ribs only[5)-7)]. The nonlinear behavior and the ultimate strength characteristics on deck-type, fixed-end, steel arch bridge systems are not clear yet. Namely, the data available to date are not sufficient to develop a direct statistical, empirical relationship that includes the fixed-end restraint effect of the arch ribs on the ultimate strength of the deck-type bridge systems.

The purpose of this paper is to discuss characteristics of the inplane ultimate strength considering the geometric and material nonlinearities of fixed-end steel arch bridge model systems that include an arch rib, a deck girder and connecting elements between them (herein termed posts) such as shown in Fig. 1, using the ultimate strength analysis originally developed by the first author[8)]. The same analysis has been adopted in Refs. 1), 3), 5), 6) and 7). Only the deck-type is considered, because this type is the most vulnerable among arch bridge types so far as the instability effects are considered. First of all, the overall

* Member of JSCE, Dr. Eng., Professor, Department of Civil Engineering, University of Ryukyu (Okinawa).
** Member of JSCE, Dr. Eng., Professor, Department of Civil Engineering, Tohoku University (Sendai).

instabilities are examined using a linear theory, a second order elastic theory and the accurate nonlinear theory by comparing their load-deflection relationships. Then, numerically studied are considerable characteristics of the incremental deflection modes of the fixed arch ribs in the bridge systems from the initial unloaded states to the ultimate states of the systems. The effects of beam-column member behavior of the arch rib between the adjacent posts in a panel are also examined. These results on the deflection modes and bending moment diagrams are used to clarify the mechanism of yielding and unloading caused by the strain reversal. Furthermore, the interaction paths between the resultant bending moment and axial thrust of the arch rib, until the ultimate state, are investigated. Next, fundamental characteristics on the ultimate strengths are briefly examined. Finally, special characteristics of local member failure (i. e., local member instability) is discussed.

The ultimate strength analysis has been carried out by the nonlinear finite element method using the modified incremental load method and the tangent stiffness approach[8]. In the numerical calculations by the nonlinear theory, the effects of finite deformation, yielding of the material, unloading caused by strain reversal and reloading, spreads of yielding, unloading and reloading zones in the cross sections and along the length of structural members, residual stress due to welding, and fixed-end effect of the arch rib are all taken into account[5)~7)]. The material behavior is idealized elastic-perfectly plastic and strain hardening is neglected in the analysis.

2. BRIDGE MODELS

Data presented herein are obtained using numerical model. The model is illustrated in Fig. 1 and its properties are also listed in the figure, where L=span length; R=rise of arch rib; h_a, h_d=depth of cross section; b_a, b_d=width of cross section; $t_{a,f}$, $t_{a,w}$, $t_{d,f}$, $t_{d,w}$=thickness of a plate composing cross section; $A_{a,f}$, $A_{a,w}$=cross-sectional area of a plate composing cross section; F_Y=yield stress level of material; subscripts a, d, f and w=structural property of arch rib, deck girder, flange and web, respectively. A single-plane, ten-panel model is employed. Although for comparison purpose, eight and six panel models are also occasionally used. The arch rib has a constant box-shaped cross section with a modified residual stress by welding[5)~7)] and is fixedly supported at the ends. The rib has a perfectly parabolic, symmetric, axial configuration, except for the cases giving different explanations from this configuration in particular. Over the rib, the deck girder is intermediately supported by the posts with hinged-hinged ends at the panel points. The girder is on rollers at the ends, however, is rigidly connected with the rib at the crown. Namely, the deck does not contribute to the longitudinal axial force. The deck girder is fabricated by constant I-shaped cross section. A distributed pattern of the residual stress in the I-shaped cross section by welding is modified as shown in Fig. 1 (i. e., a maximum stress at the welds equal to the yield stress level of material and the maximum stress in compression equal to 40 % of the yield stress). The girder has the same material with the arch rib. To avoid the failure of posts, their cross-sectional areas are decided as their squash force becomes ten times larger than a post force that will be required for equilibrium with the maximum axial thrust of the arch rib. In considering this equilibrium condition, the horizontal component of the maximum thrust is progressively evaluated as A_aF_Y, in which A_a is the cross-sectional area of an arch rib. Therefore, the cross-sectional area of a post is decided as $80\,RCA_a/L^2$, where C is the length of a panel. Furthermore, the posts are assumed to be fabricated by elastic material with the Young's modulus of 2.1×10^5 N/mm^2. Usually, the deck system consists of a reinforced concrete slab connected by shear studs to steel stringers that is turn are supported by transverse floor beams. Then the floor beams are supported by the deck girders at the panel points.

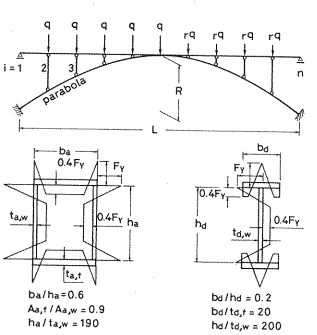

Fig. 1 Reference Bridge Model (arch geometry, loading and cross sections).

Considering this structural detail of the deck system, the model is loaded by a series of concentrated loads on the deck girder at the panel points. By refering the results of pre-examination[7], the ultimate strengths are investigated under the loading manner as shown in Fig. 1, i.e., the load acting at the each panel point on the left half of the model is q and that on the right half is rq, where r is a load intensity ratio. In all the numerical calculations the arch rib and the deck girder are respectively divided into 60 segments with equal length along the span. By dividing the cross sections of the arch rib into 36 segments and the deck girder into 27 segments the elements of tangent stiffness matrix are evaluated numerically. The structural parameters and their ranges are selected in the study as given below;

$$\left.\begin{array}{l} R/L=0.1\sim0.3\ ;\ \lambda_T=100\sim300 \quad ;\ I_d/I_a=0.1\sim10\ ; \\ r=0\sim0.99 \quad ;\ E/F_Y=457\sim875\ ;\ E=2.1\times10^5\ \mathrm{N/mm^2} \end{array}\right\} \cdots\cdots (1)$$

where λ_T is the slenderness ratio of the entire structural system of the arch bridge and is defined by the ratio of the curvilinear length of the arch axis to the square root of $(I_a+I_d)/A_a$; I_a or I_d is the second moment of area; and E is the Young's modulus. The slenderness ratio of an arch rib itself is evaluated as

$$\lambda_a=\lambda_T\sqrt{1+I_d/I_a} \cdots\cdots (2)$$

The ranges of these parameters are generally within found in steel arch bridges.

3. RESULTS OF STUDY

(1) Deflection behavior

Some selected results for dimensionless loads, q/q_p, versus total vertical deflections, v/L, at a quarter point of an arch rib with fixed-end restraints and stiffened by a deck girder ($I_d/I_a=1.0$), until the ultimate states for $r=0.5$ and 0.99, are shown in Fig. 2 by solid curves. In what follows, the applied load is nondimensionalized by dividing it by q_p. This load, when applied at all panel points, will cause full yielding at the springing of arch rib under axial thrust only[5)~7)]. It is given by:

$$q_p=\frac{A_aF_Y}{\sqrt{\left\{\frac{n-2}{2}\right\}^2+\left\{\sum_{i=1}^{n}\frac{5}{8}\frac{L}{R}\,l_1l_2(l_1^2+3\,l_1l_2+l_2^2)\right\}^2}} \cdots\cdots (3)$$

in which n=number of panel points including end-supports, $l_1=(i-1)/(n-1)$, $l_2=1-l_1$, and i=order of panel point (Fig. 1). It can be seen from this figure that the deflection at the ultimate state greatly increases with the increased lack of symmetry of the load. The results of the elastic instability analysis are also shown as the dashed curves for comparison purpose, in which the geometric nonlinearity produced by prebuckling deformation is only taken into account. The elastic analysis shows that the maximum load, $q_{\max,\mathrm{elastic}}$ does not change with the value of r very much. A similar conclusion was arrived at in Ref. 7) on the elastic behavior of fixed parabolic arch rib only. As is evident from this figure, the instability solution based on the elastic theory overestimates the ultimate strength of the arch bridge system by a large amount. This fact clearly represents that the reduction in the stiffness brought by the material nonlinearity

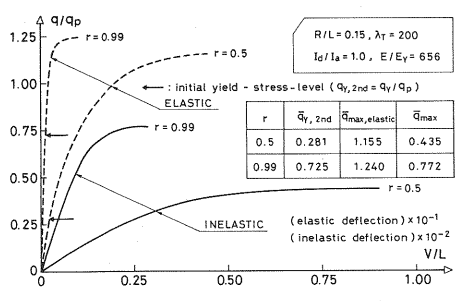

r	$\bar{q}_{Y,2nd}$	$\bar{q}_{\max,\mathrm{elastic}}$	$\bar{q}_{\max}$
0.5	0.281	1.155	0.435
0.99	0.725	1.240	0.772

Fig. 2 Load-Vertical Deflection at Quarter Point of Arch Rib.

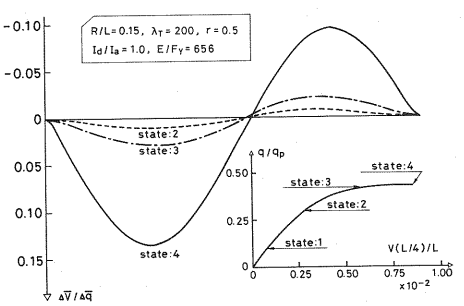

Fig. 3 Incremental Vertical Deflection Mode at Each Loading Step (for $r=0.5$).

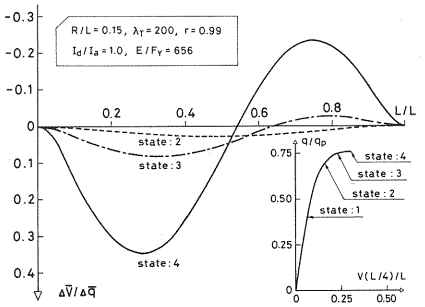

Fig. 4 Incremental Vertical Deflection Mode at Each Loading Step (for $r=0.99$).

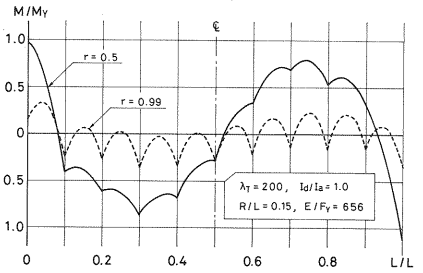

Fig. 5 Moment Diagram of Arch Rib at the Ultimate State.

considerably exerts influence on the ultimate strength.

In calculations that follow, a quasi-symmetric loading ($r=0.99$) is adopted instead of the parfectly symmetric loading ($r=1$) to avoid convergence problems and to consider ideally the effects of initial geometric imperfections. Figs. 3 and 4 show typical nondimensional forms of incremental vertical deflections of the arch rib along the bridge span ($I_d/I_a=1.0$, $\lambda_T=200$) from low level loading states to the ultimate states for $r=0.5$ and 0.99, respectively. Herein it is termed as incremental deflection mode and given by dividing the nondimensional incremental deflection ($\Delta\overline{v}=\Delta v/L$) by the dimensionless incremental load intensity ($\Delta\overline{q}=\Delta q/q_p$). From Fig. 3, it is obvious that the incremental deflection mode for each loading level under asymmetric loading ($r=0.5$) is the second order mode, in which the bending deformation is distinguished for the arch rib (bending deformation mode), until the ultimate state. On the contrary, from Fig. 4, under the quasi-symmetric loading ($r=0.99$) the incremental deflection mode for low loading level is seen to be the first order mode, in which the shortening deformation is distinguished (shortening deformation mode) because of enough flexural stiffness that the arch rib cross section exhibits against the low axial thrust. In this case the bending moment becomes negligible for the arch rib. However, when the axial thrust becomes relatively higher (just prior to the ultimate state) the incremental deflection mode changes to the bending deformation mode. Thus, the so-called inelastic instability phenomenon appears. The reasons for this instability phenomenon might be explained as follows : the flexural stiffness of the arch rib is considerably reduced along the entire arch rib due to the high axial thrust at just prior to the ultimate state. Therefore the bending moment, which was negligible under the low loading level, becomes relatively considerable. As the result, the bending deflection (anti-symmetric instability deflection mode) becomes dominant at the ultimate states of the arch ribs, eventually. The two modes on the deflection progress clearly show overall collapse configuration. Hereafter, this kind of collapse is studied except for discussions on local member failures.

(2) Internal force behavior

Fig. 5 shows internal moment diagrams of the arch rib along the bridge span ($I_d/I_a=1.0$, $\lambda_T=200$) for $r=0.5$ and 0.99 at the ultimate states (i.e., the state 4 as shown in the insets of Figs. 3 and 4). The internal moment is nondimensionalized by dividing it by the yield bending moment M_Y and plotted on the ordinate : the abscissa denotes the longitudinal coordinate set along the bridge span nondimensionalized by the span length. From Fig. 5 it can be understood that the arch rib in the deck type bridge system locally shows a beam-column member behavior in a panel with initial out-of-straightness from a line connecting with adjacent post-locations over a panel interval. Then, this initial out-of-straightness causes the arch rib an additional bending moment (hereafter, this behavior will be termed beam-column effect). If this beam-column model is illustrated as a free body diagram from the arch rib, it is idealized that the model is supported at the panel points (i.e., at the model ends) by so-called intermediate support-function provided by the posts and has rotation-springs at the model ends provided from the arch rib member over the

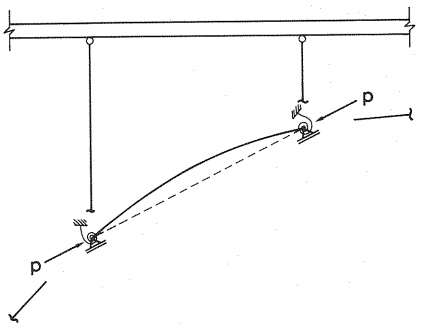

Fig. 6 A Beam-Column Model as a Free Body Diagram from Arch Rib.

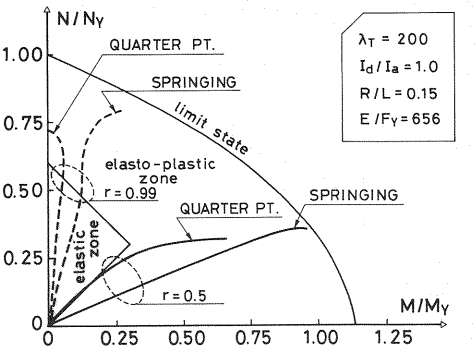

Fig. 7 Variation of Axial Thrust and Bending Moment.

adjacent panels as shown in Fig. 6.

It can be seen from Fig. 5 that this beam-column effect is more remarkable when the quasi-symmetric load is applied, because it causes high axial forces for the modeled members. The resultant bending moment versus axial thrust relationships at the quarter and center points of arch rib are given in Fig. 7 for various values of r. In this figure, the axial thrust plotted on the ordinate is given in nondimensional form by dividing it by the squash thrust N_Y $(=A_aF_Y)$ of the cross section, and the bending moment plotted on the absissa is nondimensionalized by the yield bending moment. It can be seen from Fig. 7 that the resultant bending moment under the symmetric loading increases continuously with the axial thrust showing normally nonlinear behavior until the ultimate state is reached. On the other hand, the bending moment on the quasi-symmetric loading process becomes smaller, showing nonlinear behavior, as the axial thrust increases. This phenomenon might be also explained by the beam-column behavior of the arch rib between the posts. Namely, the flexural stiffnesses of the beam-column model elements composing the arch rib are markedly reduced by the presence of the high axial compression under the quasi-symmetric loading[8]. Therefore, the bending moment that results in the arch rib is also reduced with increase of the axial thrust.

Figs. 8 (a) and (b) show the spread of yielding and unloading zones in the cross section of the deck girder and the arch rib $(I_d/I_a=1.0,\ \lambda_T=200)$ and along their longitudinal axes for $r=0.5$ and 0.99, respectively, corresponding to the load level of the state 4 (the ultimate state) as shown in the inset of Figs. 3 and 4. The locations of the posts are indicated by dushed lines in the figures. It can be observed that the spread of yielding zones shown in Fig. 8 (a) corresponds to the incremental deflection mode for $r=$

Table 1 Ultimate Strengths of Deck-Type Fixed-End Arch Bridge Systems Compared with the Elastic Critical Loads.

r	q_{max}/q_p	$q_{max,elastic}/q_p$	$q_{Y,2nt}/q_p$	$q_{Y,1st}/q_p$	q_{buckle}/q_p
0.5	0.435	1.155	0.281	0.317	1.486
0.99	0.772	1.240	0.725	0.743	

Note: $R/L=0.15, \lambda_T=200, I_d/I_a=1.0, E/F_Y=656$

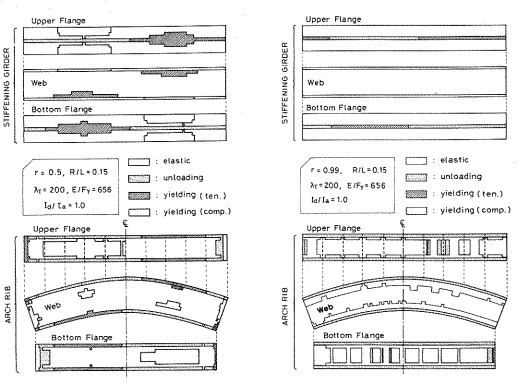

(a) for $r=0.5$ (b) for $r=0.99$

Fig. 8 Spreads of Yielding and Unloading Zones.

0.5, i.e., the bending deformation mode shown in Fig. 3. On the other hand, it can be understood from the results in Fig. 8(b) that the yielding zones, under the quasi-symmetric loading ($r=0.99$) are, broadly speaking, entirely spread out in the arch rib by the extremely high axial thrust. Furthermore, examined in detail, it is observed that the intermediate support effect brought by the posts causes unique yielding zones partially at the post-locations.

(3) Ultimate strength behavior

Selected results on the ultimate strength of the deck-type, fixed-end, arch bridge system ($\lambda_T=200$, $R/L=0.15$, $E/F_Y=656$) are tabulated in Table 1 for $r=0.5$ and 0.99 with the elastic critical loads. In the table, q_{max} indicates the true maximum load carrying capacity (ultimate strength), $q_{max,elastic}$ means the maximum load obtained by the elastic instability analysis, q_{buckle} is the linear bifurcation buckling load determined by the Japanese Highway Bridge Specification[9] in which the load is specified by the parameters of R/L and λ_T, $q_{Y,2nd}$ is the elastic limit load determined by the 2nd-order elastic analysis, i.e., the load level that gives the initiation of material yield in the structural system (residual stress not considered) and also shown in Fig. 2 by the symbol of arrows, and $q_{Y,1st}$ is the elastic limit load calculated by the conventional 1st-order elastic analysis. The $q_{max,elastic}$ does not change with the value of r very much. Essentially, the linear bifurcation buckling load should be nearly equal to the elastic maximum load obtained by the elastic instability analysis for $r=0.99$[5),6)]. However, the specified q_{buckle} is 20 % larger than the $q_{max,elastic}$ for $r=0.99$. As obvious from the results by the elastic instability analysis, neither of the buckling load and the maximum load evaluates correctly the ultimate strength. Moreover, the elastic limit load is not able to evaluate the ultimate strength even though by using the 2nd-order analysis. Typical results of the ultimate strength, q_{max}, and the elastic limit determined by the 1st-order analysis, $q_{Y,1st}$ that is ordinarily used in design practical to account for the allowable stress, are widely given in Table 2, where the results of the hinged arch bridge systems having identical, geometric and material properties and loading condition are also tabulated for comparison purpose. In the traditional approach to design, the 1st-order elastic limit of a structure has been the basis for the development of design methods. However, from the calculated results in the table, the magnitude of discrepancy between the ultimate strength and the elastic limit, $(q_{max}-q_{Y,1st})$, to the q_{max} for the twenty seven cases are scattering, in term of percentage, from −72 % to +52 % in the fixed arch bridge systems and from −259 % to +16 % in the hinged ones. The average of the absolute magnitude is 31 % for the fixed systems and 45 % for the hinged ones. The elastic limit approach leads to quite difference from the ultimate strength for the arch bridge system. The q_{buckle} is also tabulated in the space for $r=0.99$. For instability of arches, specified

Table 2 Ultimate Strengths of Deck-Type Fixed-End Arch Bridge Systems Compared with those of 2-Hinged Systems.

r	Arch Type	I_d/I_a	$\lambda_T=100$			$\lambda_T=200$			$\lambda_T=200$		
			q_{max}/q_p	$q_{Y,1st}/q_p$	q_{buckle}/q_p	q_{max}/q_p	$q_{Y,1st}/q_p$	q_{buckle}/q_p	q_{max}/q_p	$q_{Y,1st}/q_p$	q_{buckle}/q_p
0	Fixed	0	0.672	0.414		0.340	0.236		0.207	0.164	
		1	0.693	0.342		0.326	0.188		0.192	0.127	
		10	0.754	0.365		0.317	0.188		0.183	0.128	
	Hinged	0	0.467	0.428		0.213	0.237		0.125	0.164	
		1	0.561	0.513		0.247	0.268		0.142	0.178	
		10	0.699	0.740		0.286	0.362		0.162	0.240	
0.5	Fixed	0	0.795	0.586		0.459	0.381		0.283	0.283	
		1	0.845	0.463		0.435	0.317		0.249	0.219	
		10	0.918	0.542		0.409	0.295		0.220	0.207	
	Hinged	0	0.607	0.618		0.288	0.391		0.159	0.285	
		1	0.739	0.648		0.321	0.441		0.173	0.330	
		10	0.931	0.778		0.369	0.549		0.195	0.424	
0.99	Fixed	0	0.961	0.986	0.944	0.801	0.969	1.486	0.555	0.952	0.660
		1	0.930	0.690		0.772	0.743		0.480	0.702	
		10	0.854	0.709		0.653	0.577		0.333	0.483	
	Hinged	0	0.837	1.000	2.730	0.538	1.000	0.684	0.280	1.000	0.304
		1	0.915	0.866		0.577	0.754		0.289	0.668	
		10	0.800	0.717		0.545	0.551		0.293	0.450	

Note: $R/L=0.15, E/F_Y=656$

allowable stresses are still widely based on the elastic buckling approach[10),11)]. It is, however, obvious from the table that the elastic buckling approach can not estimate correctly the actual instability of arches, i. e., the instability phenomenon under the geometric and material nonlinear effects. It can be clearly understood from the table that the ultimate strength decreases with the increased lack of symmetry of the loading. Generally, for a certain value of λ_T the ultimate strength of deck-type fixed arch bridge systems for the most any case increases with decrease of I_d/I_a, while that of hinged one increases with I_d/I_a. It means that the capacity of resistance to the failure provided in the deck type arch bridge system by fixing supports of the arch rib is higher than that by making flexural stiffness of the deck-girder higher.

Fig. 9 shows the variation of the ultimate strengths, q_{max}/q_p as a function of the slenderness ratio of the deck-type, fixed-end arch bridge systems, λ_T, for various values of the flexural stiffness ratios, I_d/I_a and the load intensity ratios, r. As is obvious from this figure, the ultimate strength decreases with the slenderness ratio and it should be one of the important parameters to predict the ultimate strength. In the case of the quasi-symmetric loading a certain difference between the ultimate strengths for $I_d/I_a=0.1$ (a Lohse-type) and for $I_d/I_a=10$ (a Langer-type) arises, while in the case of the asymmetric loading there is no significant difference between the two. Typical results for the influence of rise-to-span ratio on the ultimate strengths of the arch bridge systems with a slenderness ratio of the bridge system, $\lambda_T=200$, are shown in Fig. 10 for various values of the flexural stiffness ratios and the load intensity ratio. It can be considered from the figure that the ultimate strength, expressed in the nondimensional ultimate load form with, q_p, given by Eq. (3), is not affected very much by the rise-to-span ratio of the arch rib within its structural parameter ranges adopted herein, Eq. (1). Some selected results on the relationship between the nondimensional ultimate load intensity, q_{max}/q_p, and the yield stress level of material expressed by a nondimensional form, E/F_Y, are shown in Fig. 11. Similar studies for the arch bridge systems with different slenderness ratios also shows almost same tendency as the results shown in Fig. 11. Namely, the data analyzed herein show that the effect of the yield stress level on the nondimensionalized ultimate load intensity is not significant, regardless of the values λ_T, I_d/I_a, R/L and r.

(4) Local failure behavior

A slender arch rib with long panel-intervals between the posts in deck-type arch bridge system under high axial loading raises a member failure in a panel possibly, i. e., local member failure before the overall instability of the bridge system occurs, because of severe response of the beam-column behavior as was mentioned previously. Fig. 12 shows, after magnification, typically analyzed result on the appearance of progress in the local member failure mode until the ultimate state is reached. In this figure, the ordinate indicates an nondimensional form of vertical deflection by dividing it by the span length, v/L, and the abscissa denotes the nondimensionalized longitudinal coordinate set along the bridge span, X/L. The fixed-end arch bridge adopted in this calculation is, so-called, a Langer-Type decked system ($I_d/I_a=10$). It has six panels of equal interval along the span under the quasi-symmetric loading and has the structural properties for $E/F_Y=656$, $R/L=0.15$ and $\lambda_T=200$. It can be seen from the figure that the local member failure arises originally in the first panel countered out from the springing as well known.

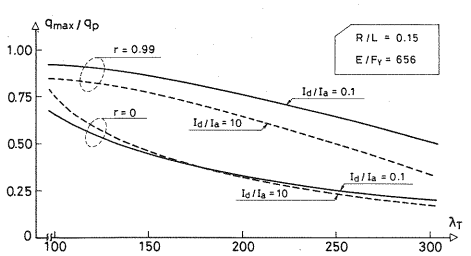

Fig. 9 Variation of the Ultimate Load Intensity as a Function of Slenderness Ratio.

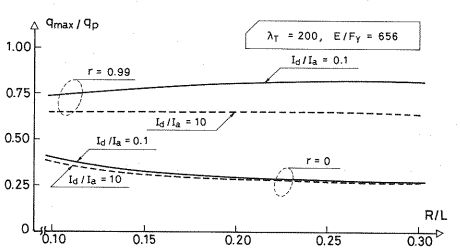

Fig. 10 Variation of the Ultimate Load Intensity as a Function of Rise-to-Span Ratio.

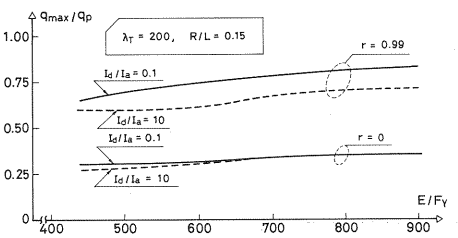

Fig. 11 Variation of the Ultimate Load Intensity as a Function of Yield Stress Level of Material.

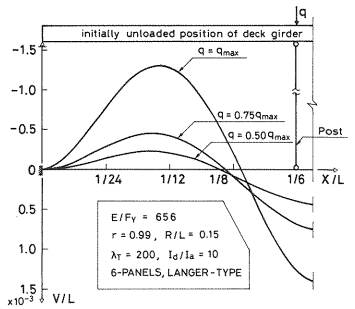

Fig. 12 Appearance of Progress in Local Member Failure Mode until the Ultimate State.

Table 3 Influence of Panel Number on the Ultimate Strength of Deck-Type Fixed-End Arch Bridge Systems (for various values of λ_T and I_d/I_a).

λ_T	I_d/I_a	Panel Number				
		6			8	10
		parabolic	polinomial		parabolic	parabolic
			imperfection	no imperfection		
100	0.1	0.846			0.905	0.914
	10	0.672 (L)	0.832 (L)	0.900	0.780 (L)	0.854
150	0.1	0.783			0.844	0.875
	10	0.523 (L)	0.696 (L)	0.728	0.676 (L)	0.766
200	0.1	0.703			0.748	0.768
	10	0.402 (L)	0.526 (L)	0.536	0.566 (L)	0.635
300	0.1	0.469			0.497	0.510
	10	0.232 (L)	0.264 (L)	0.266	0.304 (L)	0.333

Note: $r = 0.99, R/L = 0.15, E/F_Y = 656, (L) = local member failure$

Table 3 summarizes the ultimate strengths of the Lohse-Type (I_d/I_a=0.1) and the Langer-Type (I_d/I_a =10) under the quasi-symmetric loading for various values of panel number and λ_T. The panel numbers adopted are 6, 8 and 10, respectively. In the table (L) expresses ultimate strength influenced by local member failure of arch rib, and the other values show overall instability, i.e., ultimate strength not influenced by local member failure. From the results in the table, it can be understood that the possibility of the local member failure becomes high as the number of panels or the slenderness ratio of the bridge system or both of them decrease. Similar studies on the local member failure are also performed herein for various values of the load intensity ratio, r, and the flexural stiffness ratio, I_d/I_a. The results show that the local member failure is apt to arise as the load intensity ratio, r, is merged to unity and the flexural stiffness of the arch rib becomes smaller than that of the deck girder.

For 6-panel system, shapes of arch ribs that correspond to a sixth-order polynomial with and without the initial crookedness, as shown in Fig. 13, are also examined for comparison purpose. Their shapes are symmetric with respect to the crown. The crookedness is given by a sinusoidal between the panel intervals shown in Fig. 13. The corners of the sixth-order polynomial locating the posts are found by the coordinates of a parabolic function as shown in the inset of Fig. 13. Theie examined results are also shown in Table 3. It can be understood from the results that the ultimate strength of the Langer-Type composed of six panels having the parabolic arch rib are characterized by the local member failure and those of the Lohse-Type are characterized by the overall instability in the range of the slenderness ratios of the bridge systems discussed herein (λ_T=100~300). The local member failures are also induced for the sixth-order polinomial arch ribs with the initial crookedness in the Langer-Type system, while without the crookedness they are not. The ultimate strength of the Langer-Type composed of six panels having the parabolic arch rib is higher than that having the polynomial arch rib with the crookedness. It seems to cause this discrepancy between the two that the initial crookedness of the aforementioned beam-column model in the parabolic arch is a degree of $L/250$ at a center of the model, while the crookedness adopted in

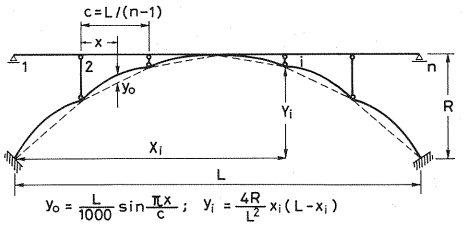

Fig. 13 Six Panel Model with Porinomial Arch Axis Configuration.

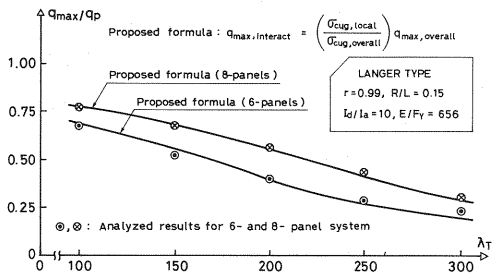

Fig. 14 Influence of Local Member Failure on the Ultimate Load Intensity.

the polinomial arch rib is $L/1\,000$.

The analytical study of the Langer-Type arch bridge system with various values of panel numbers shows that the decrease in strength is due primarily to the local member failure of the beam-column model at the end panel. A simple way of incorporating this effect is to use the strength reduction factor, ϕ, that evaluates interaction of the local and overall instability. The coefficient, ϕ, could be evaluated by the following equation;

$$\phi=\sigma_{cug,local}/\sigma_{cug,overall} \quad \cdots\cdots (4)$$

where $\sigma_{cug,local}$=strength of the beam-column model at the end panel of arch rib with the local member failure and $\sigma_{cug,overall}$=strength of the beam-column model at the end panel of standard arch rib in which the local member failure does not occur until the ultimate state is reached (i.e., the ultimate strength is characterized by so-called overall instability). The Langer-Type arch bridge system with 10 panels is herein adopted as the standard one because only overall instability occurs to this system. The interactive ultimate strength, $q_{max,interact}$, can therefore be determined as follows;

$$q_{max,interact}=\phi q_{max,overall} \quad \cdots\cdots (5)$$

where $q_{max,overall}$=the ultimate load intensity of the standard arch bridge system. Provided that, the arch system established by the ultimate strength of $q_{max,interact}$ has all identical structural properties with the abovementioned standard one, except the slenderness ratio of the beam-column model.

The numerical results obtained from this study make the practical formulation of ϕ. The first step is to establish the formulation of $\sigma_{cug,overall}$. The $\sigma_{cug,overall}$ for the standard arch rib was computed using the same computer program as used herein. In analyzing the beam-column, it was modified as fixed-hinged boundary conditions and given the initial crookedness corresponding to the parabolic configulation of the standard arch rib. Then, the axial load was applied to the initially bent column. By applying regression analysis on statistics to the computed results, a prediction formula for $\sigma_{cug,overall}$ can be obtained as follows;

$$\sigma_{cug,overall}=(1.194-0.218\,\bar{\lambda}_T)F_Y \quad \cdots\cdots (6)$$

where $\bar{\lambda}_T=(\lambda_T/\pi)\sqrt{F_Y/E}$. It is proposed to use the same $\sigma_{cug,overall}$ to evaluate ϕ defined by Eq. (4). The second step is to establish the formulation of $\sigma_{cug,local}$. The $\sigma_{cug,local}$ is evaluated by Eqs. (4) and (5) as follows;

$$\sigma_{cug,local}=\phi\sigma_{cug,overall}=\sigma_{cug,overall}\frac{q_{max,interact}}{q_{max,overall}} \quad \cdots\cdots (7)$$

By substituting the analyzed results of $q_{max,interact}$ for the 6- and 8-panel arch systems and of $q_{max,overall}$ and Eq. (6) into Eq. (7), the $\sigma_{cug,local}$, in which the interactive effect is included, is given. On the other hand, since $\sigma_{cug,local}$ is the strength of beam-column model at the end panel of arch rib with local member failure, the $\sigma_{cug,local}$ may be evaluated by the column-strength-formula as follows;

$$\left.\begin{aligned}\sigma_{cug,local}&=F_Y && ;\text{for } \bar{\lambda}\leq 0.2\\ &=F_Y[1.0-0.545(\bar{\lambda}-0.2)] && ;\text{for } 0.2<\bar{\lambda}\leq 1.0\\ &=F_Y/(0.733+\bar{\lambda}^2) && ;\text{for } 1.0<\bar{\lambda}\end{aligned}\right\} \quad \cdots\cdots (8)$$

$$\bar{\lambda}=(k_e l_a/r_a)(1/\pi)\sqrt{F_Y/E} \quad (9)$$

where l_a=axial length of the beam-column model at the end panel, r_a=radius of gyration of the arch rib cross section. Substituting the value of Eq. (7) and Eq. (9) into Eq. (8), the coefficient k_e is obtained. Eventually the effects of the boundary condition, the initial crookedness and the interaction of overall and local instability are included in the k_e. By applying the regression analysis to the values of k_e obtained herein, a prediction formula for k_e can be derived as follows;

$$k_e=0.900 \quad (10)$$

It is proposed to use the $\sigma_{cug,local}$ formulated by Eqs. (8), (9) and (10) to evaluate ϕ defined by Eq. (4). The accuracy of using the strength reduction factor defined by Eqs. (4), (6), (8), (9) and (10) in evaluating the interactive strengths of deck type fixed end arch bridge systems is illustrated in Fig. 14. The solid curves show the interactive strength evaluated by Eq. (5), in which the 10-panel system is adopted as the standard arch bridge and it is analyzed by the ultimate strength approach. The circular marks indicate the q_{max}/q_p for 8- and 6-panel systems that are also calculated by the ultimate strength analysis. The correlations are considered satisfactory for design purpose. It may be concluded that the interactive strength concept proposed herein gives results that are sufficiently accurate for practical applications.

4. CONCLUSIONS

For fixed-end steel arch systems with deck type girder, the function of the deck girder, the fixed-end restraint behavior of the arch rib and the ultimate strength of the bridge system characterized by the overall instability and the local member failure have been studied by an accurate nonlinear finite element approach in the inelastic and the finite deformation ranges. The parametric studies have been performed in the ranges of the structural parameters that are generally within those found in the arch bridges. Based on this study the following conclusions can be drawn chiefly:

(1) The deformation behavior until the instability state is reached to the arch bridge system has been studied by the linear theory, the second order elastic theory and the ultimate strength approach. It is shown that the instability solutions based on the elastic theories overestimate considerably the true ultimate load carrying capacity, i.e., ultimate strength. The elastic limit load is not able to evaluate the ultimate strength, even though by using the 2nd-order analysis.

(2) The type of collapse conditions has been examined with the help of the incremental deflection mode at several loading states starting from a low level loading state to the ultimate state. The bridge systems have two kinds of overall collapse conditions; one shows the nonlinear bending deformation-response and the other the inelastic instability phenomenon. Eventually, the bending deformation mode (antisymmetric mode) becomes dominant at the ultimate states of the arch bridge systems.

(3) The parabolic arch ribs show a sort of beam-column model behavior with initial out-of-straightness from a line connecting with adjacent post-locations over a panel interval. This beam-column behavior becomes more remarkable, when the quasi-symmetric load is applied because it causes high axial loading to the model.

(4) The unique interaction between the resultant axial thrust and bending moment causing to the arch ribs has been examined. It has been revealed that the bending moment producing between two posts adjacent to each other becomes smaller, showing nonlinear behavior, as the axial thrust increases on the quasi-symmetric loading process.

(5) The results on the spread of yielding zones clearly show how the flexural stiffness is reduced by the asymmetric or quasi-symmetric loading. The spread of yielding zones corresponds to the incremental deflection mode. The restraining bending moment-components brought by the intermediate post-supports cause partially unique yielding zones at the post locations in the arch rib under the quasi-symmetric loading.

(6) The ultimate strength decreases with increased lack of symmetry of the loading or increase of the slenderness ratio of the bridge system λ_T or both of them. The ultimate strength, expressed in the nondimensional load form with, q_p, given by Eq. (3), is not affected very much by the rise-to-span ratio of the arch rib in the practical cases. The effect of the yield stress level on the nondimensionalized ultimate load intensity is not significant, regardless of the values of λ_T, I_d/I_a, R/L and r. These fundamental qualitative characteristics of the ultimate strengths are the same as those of two-hinged steel arch bridge systems.

(7) Generally, for a certain value of λ_T the ultimate strength of the fixed arch bridge system for the most any case investigated herein increases with decrease of I_d/I_a while that of the hinged one increases with I_d/I_a. For the deck-type systems having arch ribs with certain, flexural and contractive stiffnesses, fixing the end-supports of the arch ribs is, speaking from view point of their ultimate strengths, more effective than making flexural stiffness of the deck girders in the two-hinged system higher.

(8) The possibility of the local member failure becomes high as the number of panel decreases and the load intensity ratio, r, is merged to unity. In addition, the local member failure is apt to arise as the flexural stiffness of the arch rib becomes smaller than that of the deck girder and the slenderness ratio of the bridge system decreases.

(9) The local member failure is induced for the sixth-order polinomial arch rib with an initial crookedness (sinusoidal crookedness with $L/1\,000$ peak) in a Langer-Type ($I_d/I_a=10$). However, the Langer-Type having the polinomial rib without the initial crookedness does not occur the local member failure in the range of the slenderness ratio of the bridge system, $\lambda_T=100\sim300$.

(10) The ultimate strength of the Langer-Type composed of six panels having the parabolic arch rib is lower than that having the polinomial rib with the initial crookedness. The cause for the discrepancy between the two seems to be that the initial crookedness of the beam-column model over a panel interval in the parabolic arch rib is a degree of $L/250$ at the center of the model length, while the crookedness adopted in the polinomial arch is $L/1\,000$.

(11) It can be proposed to use the strength reduction factor ϕ formulated by Eqs. (4), (6), (8), (9) and (10) to evaluate the interaction of the local member failure and the overall instability of deck type fixed end arch bridge with parabolic axial configuration. The practical formula for evaluating the interactive strength, $q_{\max,\text{interact}}$, can therefore be defined by $q_{\max,\text{interact}}=\phi q_{\max,\text{overall}}$.

From these results it can be seen that implementation of a design method for the deck-type arch bridge systems based on the abovementioned ultimate strength characteristics is desirable. Work on development of such ultimate strength design approach for the arch bridge system is in progress by the writers.

ACKNOWLEDGEMENTS

The writers wish to thank Messrs. N. Tokashiki, Y. Arizumi, and M. Hayase of the Department of Civil Engineering at University of Ryukyu for drawings, some primary parts of the computer runs and typings.

NOTATION

The following symbols are used in this paper;

A_a =cross-sectional area of arch rib;
$A_{a,f}$, $A_{a,w}$ =cross-sectional area of plate composing cross section;
c =length of panel;
E, F_Y =Young's modulus and yield stress level of material;
I_a, I_d =second moment of area;
M_Y, N_Y =yield moment and squash thrust;
L, R =span and rise of arch rib

X =longitudinal coordinate set along span;
b_a, b_d =width of cross section;
h_a, h_d =depth of cross section;
i, n =order of panel point and number of panel points;
l_a =axial length of arch rib in end panel;
q =a concentrated load applied at a panel point of deck girder;
q_p =full plastic load;
$q_{Y,1st}$ or $q_{Y,2nd}$ =elastic limit load calculated by 1st or 2nd order elastic analysis;
q_{max} =maximum load carrying capacity (ultimate strength);
$q_{max,elastic}$ =maximum load obtained by elastic instability analysis;
q_{buckle} =linear bifurcation buckling load determined by the Japanese Highway Bridge Specifications;
$q_{max,interact}$ =interactive strength of local failure and overall instability;
$q_{max,overall}$ =ultimate load intensity of the standard arch bridge system;
r =load intensity ratio;
r_a =radius of gyration;
$t_{a,f}$, $t_{a,w}$, $t_{d,f}$, $t_{d,w}$ =thickness of a plate composing cross section;
v =vertical displacement;
ϕ =strength reduction factor evaluating effect of local member failure;
$\sigma_{cug,local}$ =strength of beam-column model at the end panel of arch rib with the local member failure;
$\sigma_{cug,overall}$ =strength of beam-column model at the end panel of arch rib in the standard arch bridge system;
λ_T, λ_a, $\bar{\lambda}$ =slenderness ratio of arch bridge system, slenderness ratio of arch rib and slenderness ratio parameter of beam-column model;
Subscript a, d, f or w =structural property of arch rib, deck girder, flange or web.

REFERENCES

1) Kuranishi, S., Sato, T. and Otsuki, M. : Load Carrying Capacity of Two Hinged Steel Arch Bridges with Stiffening Deck, Proc. of JSCE, No. 300, pp. 121-130, 1980.
2) Shinke, T., Zui, H. and Nakagawa, T. : In-plane Load Carrying Capacity of 2-Hinged Arches with a Stiffening Girder, Proc. of JSCE, No. 301, pp. 47-59, 1980 (in Japanese).
3) Yabuki, T. and Kuranishi, S. : Ultimate Strength Design of Steel Arch Bridge Structures, IABSE Proc. P-84/85, International Association for Bridge and Structural Engineering, pp. 57-64, 1985.
4) Wen, R. K. and Medallah, K. : Elastic Stability of Deck-Type Arch Bridges, Journal of Structural Engineering, ASCE, Vol. 113, No. 4, pp. 757-768, 1987.
5) Yabuki, T., Vinnakota, S. and Kuranishi, S. : Fixed-End Restraint Effect on Steel Arch Strength, Journal of Structural Engineering, ASCE, Vol. 112, No. 4, pp. 653-664, 1986.
6) Yabuki, T., Lu, L. W. and Kuranishi, S. : An Ultimate Strength Design Aid for Fixed-End Steel Arches Under Vertical Loads, Proc. of JSCE, Structural Eng./Earthquake Eng., Vol. 4, No. 1, pp. 115s-123s, 1987.
7) Yabuki, T. and Kuranishi, S. : Ultimate Strength Design Provisions for Fixed-End Steel Arches with Variable Cross-Sections, Proc. of JSCE, Structural Eng./Earthquake Eng., Vol. 5, No. 1, pp. 81s-87s, 1988.
8) Kuranishi, S. and Yabuki, T. : Ultimate In-plane Strength of 2-Hinged Steel Arches Subjected to Lateral Loads, Proc. of JSCE, No. 272, pp. 1-12, April, 1978 (in Japanese).
9) Japanese Road Association : Specification for Highway Steel Bridges, 1980 (in Japanese).
10) American Association of State Highway and Transportation Officials : Standard Specifications for Highway Bridges, 13th, edition 1983.
11) Stabilitätsfälle Knicken von Stäben und Stabwerken, Din 18800 Teil 2, Norm-Vorlage März, 1986.
12) Committee on Steel Structures, JSCE : Design Code for Steel Structures—PART A ; Structures in General—.

(Received May 8 1989)